Seeing Galaxies through Thick and Thin. I. Optical Measures in Overlapping Galaxies

Raymond E. White III – University of Alabama

William C. Keel – University of Alabama

Christopher J. Conselice – University of Chicago

Citation of published version:

White III, R., Keel, W., Conselice, C. (2000): Seeing Galaxies through Thick and Thin. I. Optical Measures in Overlapping Galaxies. *The Astrophysical Journal*, 542(2).
DOI: https://doi.org/10.1086/317011

THE ASTROPHYSICAL JOURNAL, 542:761–778, 2000 October 20

SEEING GALAXIES THROUGH THICK AND THIN. I. OPTICAL OPACITY MEASURES IN OVERLAPPING GALAXIES[1]

RAYMOND E. WHITE III[2,3,4]
NASA Goddard Space Flight Center, Laboratory for High Energy Astrophysics, Code 662, Greenbelt, MD 20771; and Department of Physics and Astronomy, University of Alabama, Tuscaloosa, AL 35487-0324
WILLIAM C. KEEL[2,3,4]
Department of Physics and Astronomy, University of Alabama, Tuscaloosa, AL 35487-0324
AND
CHRISTOPHER J. CONSELICE[3,5,6]
Department of Astronomy and Astrophysics, University of Chicago, Chicago, IL 60637
Received 2000 April 28; accepted 2000 May 24

ABSTRACT

We describe the use of partially overlapping galaxies to provide direct measurements of the effective absorption in galaxy disks, independent of assumptions about internal disk structure. The nonoverlapping parts of the galaxies and symmetry considerations are used to reconstruct, via differential photometry, how much background galaxy light is lost in passing through the foreground disks. Extensive catalog searches and follow-up imaging yield ~15–25 nearby galaxy pairs suitable for varying degrees of our analysis; 11 of the best such examples are presented here. From these pairs, we find that interarm extinction is modest, declining from $A_B \sim 1$ mag at $0.3R_{25}^B$ to essentially zero by R_{25}^B; the interarm dust has a scale length consistent with that of the disk starlight. In contrast, dust in spiral arms and resonance rings may be optically thick ($A_B > 2$) at virtually any radius. Some disks have flatter extinction curves than the Galaxy, with $A_B/A_I \approx 1.6$; this is probably the signature of clumpy dust distributions. Even though typical spirals are not optically thick throughout their disks, where they *are* optically thick is correlated with where they are most luminous: in spiral arms and inner disks. This correlation between absorption and emission regions may account for their apparent surface brightness being only mildly dependent on inclination, erroneously indicating that spirals are generally optically thick. Taken as an ensemble, the opacities of spiral galaxies may be just great enough to significantly affect QSO counts, though not enough to cause their high-redshift cutoff.

Subject headings: dust, extinction — galaxies: ISM — galaxies: photometry — galaxies: spiral

1. INTRODUCTION

Interest in the dust content of spiral disks, particularly in its role as a source of opacity in "typical" galaxies, has been revived by several recent studies. Different aspects of this problem have been clarified by a variety of observational approaches.

The inclination surface brightness test is one of the oldest methods used to determine whether spiral galaxies are largely transparent or opaque (Holmberg 1958), and this test is still being refined (Valentijn 1990; Burstein, Haynes, & Faber 1991). An opaque spiral disk would have the same surface brightness regardless of its inclination, while a transparent disk would have a higher surface brightness when edge-on than when face-on. Applying this test to a sample of galaxies drawn from the ESO-LV catalog, Valentijn (1990) found spirals to be largely opaque. This seems counterintuitive for two reasons: (1) if spirals are opaque, then the galaxy survey used to deduce this would have been difficult to obtain, since we live in a spiral galaxy; and (2) there are also well-known examples of distant objects (galaxies, quasars, etc.) seen through foreground spiral galaxies other than the Milky Way. In a statistical reassessment of Valentijn's (1990) work, Burstein et al. (1991) concluded that Valentijn got the right answer for the wrong reason, maintaining that the result was a product of sample selection effects. Using a sample claimed to be less subject to such selection effects, Burstein et al. (1991) nonetheless found that spirals are optically thick (although not *opaque*, per se). Most recently, however, Burstein, Willick, & Courteau (1995) now find in an expanded sample that spirals are *not* so optically thick after all, since the new surface brightness sample exhibits a mild inclination dependence. Huizinga (1994) has suggested that the Valentijn (1990) result was confounded by the presence of bulge systems in the sample, the surface brightnesses of bulges being inherently more inclination independent than those of spiral disks. However, it is obvious from illustrations in Valentijn (1990) that there is a large variance in spiral surface brightnesses at a *given* inclination, which would mask a mild trend of surface brightness with inclination. This may explain why this classical method is still of interest—it gives ambiguous results!

[1] Based in part on archival observations with the NASA/ESA *Hubble Space Telescope* (*HST*) obtained at the Space Telescope Science Institute, which is operated by the Association of Universities for Research in Astronomy, Inc., under NASA contract NAS5-26555.

[2] Visiting Astronomer, Kitt Peak National Observatory, National Optical Astronomy Observatories, operated by AURA, Inc., under cooperative agreement with the National Science Foundation.

[3] Visiting Astronomer, Cerro Tololo Inter-American Observatory (CTIO), National Optical Astronomy Observatories, operated by AURA, Inc., under cooperative agreement with the National Science Foundation.

[4] Visiting Astronomer, Lowell Observatory, Flagstaff, AZ 86001.

[5] NSF REU summer student at University of Alabama.

[6] Present address: Department of Astronomy, University of Wisconsin, Madison, WI 53706.

Another approach to determining dust opacity in spiral disks is to compare radiative transfer models with observed color and surface brightness data (Disney, Davies, & Phillips 1989; Davies 1990; Witt, Thronson, & Capuano 1992). While the traditional interpretation is that we see most of the starlight, free of much reddening or obscuration (Holmberg 1958; de Vaucouleurs et al. 1991), these radiative transfer studies show that the observed color and surface brightness data do *not* require low internal extinction and can be modeled just as well by very dust-rich systems, in which the optical light is dominated by the small fraction of least-obscured stars.

Observing the kinematics of edge-on galaxies at various wavelengths offers another means for assessing absorption in disks (Bosma et al. 1992). Using a 21 cm H I rotation curve as a template, one can determine how deeply an observed rotation curve at some optical or near-infrared band probes into the disk. The two galaxies observed by Bosma et al. (1992) were shown to be largely transparent.

When seen behind foreground galaxies, the colors of quasi-stellar objects (QSOs) or the Balmer decrements of H II regions can also be used to provide crude limits on foreground reddening. James & Puxley (1993) analyzed the Balmer decrements of two H II regions projected behind the inner disk of NGC 3314, the foreground galaxy of an exactly superposed pair (first analyzed by Keel 1983); they found extinctions of $A_B \approx 1.7$ mag. However, when applied to individual QSOs or H II regions, this technique selects against high opacity regions, which would completely obscure small background objects.

Comparing images at widely disparate wavelengths such as B and K can also be used to determine the intrinsic absorption of spiral disks (Block et al. 1994). A control image is taken in a band at wavelengths long enough to be minimally affected by dust and compared to an image taken at shorter wavelengths. Some of the structure in the resulting color map can be attributed to the reddening effects of dust. Block et al. (1994) find that dust distributions tend to be very patchy and concentrated along spiral arms. However, this measurement is also sensitive to stellar population gradients and to the vertical distribution of absorbing material, since material at large z-distances will be most effective at absorbing the overall disk radiation (a fact used by Elmegreen 1980 to model the scale heights of various disk constituents as well as the dust in spirals). Furthermore, because the three-dimensional geometry is not known in detail, effects of scattering are important in the interpretation (as seen in the recent claim by Block et al. 1994 that scattering can serve to hide grand-design spiral patterns in apparently flocculent spirals).

Inspired initially by the work of Valentijn (1990), we initiated a program to determine the opacity of spiral disks *directly*, rather than statistically, by imaging foreground spirals partially projected against background galaxies. The nonoverlapping regions of a partially overlapping galaxy pair can be used to reconstruct, using purely differential photometry, how much light from the background galaxy is lost in passing through the foreground galaxy in the region of overlap. Initial results are presented in White & Keel (1992), Keel & White (1995), and White, Keel, & Conselice (1996).

This technique has recently been applied to individual systems by Berlind et al. (1997) and Pizagno & Rix (1998). This general approach was also employed by Roennback & Shaver (1997), using the distant elliptical radio galaxy (PKS 1400−181 at $z = 0.341$) seen through the disk of a nearby spiral at $z = 0.0367$ to limit the average opacity of the spiral disk. We also note that it has been applied to strongly interacting pairs, in which tidal distortion may limit generalization to the general spiral population, by Thronson, Rubin, & Ksir (1991) and Reshetnikov & Sazonova (1993).

2. METHODOLOGY

2.1. *Constructing Opacity Maps*

Our technique for constructing disk opacity maps using purely differential photometry is illustrated in Figure 1. The ideal case consists of a foreground disk (spiral) galaxy half-projected against half of a similarly sized background elliptical galaxy. For the sake of illustration, the (unobscured) surface brightness of each galaxy is taken to be constant, with F and B being the actual surface brightness values of the foreground disk and background elliptical in the overlap region, and τ is the optical depth in the disk. The observed surface brightness in the overlap region is then $\langle F + Be^{-\tau} \rangle$, where brackets are used to emphasize that this whole quantity is the observable in the overlap region and cannot be directly decomposed into its constituent components. We use symmetric counterparts from the nonoverlapping regions of the two galaxies to *estimate* F and B and denote the estimates as F' and B'. We can then construct an estimate of the optical depth, denoted τ', as follows:

$$e^{-\tau'} = \frac{\langle F + Be^{-\tau} \rangle - F'}{B'} . \quad (1)$$

Here the estimate of the foreground spiral's surface brightness, F', is first subtracted from the surface brightness of the overlap region, $\langle F + Be^{-\tau} \rangle$; this result is then divided by the estimate of the background elliptical's surface brightness, B'. This creates a map of $e^{-\tau'}$ in the overlap region.

Although it is impossible to actually do so strictly from observable quantities, it is *formally* useful to "break" $\langle F + Be^{-\tau} \rangle$, the observed surface brightness in the overlap

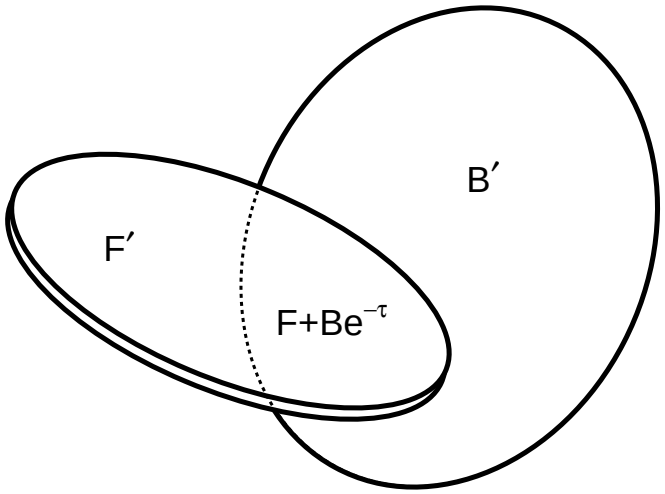

FIG. 1.—Cartoon of the ideal galaxy pair for our analysis. The light from stars in the foreground and background systems is denoted by F and B; their values in the overlap regions are estimated from the values F', B' in symmetrically located regions on the nonoverlapping sides of the galaxies.

region, into its constituent parts to assess the systematic errors of the above construction:

$$e^{-\tau'} \cong \frac{F - F'}{B'} + \frac{B}{B'} e^{-\tau} . \quad (2)$$

The systematic errors induced by departures from symmetry can be estimated from the nonoverlapping parts of the galaxies. Note that when the background galaxy has substantially higher surface brightness than the foreground galaxy ($B' \gg F, F'$), the estimate of τ is particularly insensitive to systematic errors induced by asymmetries in the foreground spiral. In this case,

$$e^{-\tau'} \approx \frac{B}{B'} e^{-\tau} , \quad (3)$$

with B/B' being especially close to unity for most ellipticals and S0 galaxies. Also, a lower limit to τ' is provided by simply dividing the overlap region by the symmetric counterpart of the background galaxy and neglecting to scrape off the emission from the foreground galaxy:

$$e^{-\tau'} < \frac{\langle F + Be^{-\tau} \rangle}{B'} \quad \Rightarrow \quad \tau' > -\ln \frac{\langle F + Be^{-\tau} \rangle}{B'} . \quad (4)$$

Depending on the inclination of the foreground galaxy, different symmetries are useful for scraping off the emission due to the foreground spiral in the overlap region: if the spiral is nearly face-on, rotation symmetry is used to swing the unprojected portion around for subtraction; if the foreground spiral is instead more edge-on, its finite disk thickness may require reflection symmetry to be used to flip the unprojected portion of the spiral over for subtraction. The opacities we determine directly are line-of-sight values, which we correct to face-on values (assuming slab geometry) by dividing by the axial ratio a/b of the foreground galaxy. If the absorbing dust resides in spheres with only $\lesssim 1$ per line of sight, then no correction is necessary.

2.2. *Methodological Advantages and Caveats*

In light of the ongoing controversy over selection effects in statistical samples and the structural assumptions needed to interpret some of the multiwavelength tests noted in § 1, there are several benefits to the direct, differential photometric approach we use to determine spiral opacities: (1) it is not subject to the selection effects that influence the statistical studies cited above; (2) there is no selection against high-opacity regions, as there is in some spectroscopic studies of small or pointlike background objects shining through foreground disks (e.g., quasars or H II regions in a background galaxy; see James and Puxley 1993); (3) our imaging technique involves only differential photometry, so calibration errors are not an issue; (4) large, contiguous areas can be analyzed, allowing average values of the opacity to be estimated (whereas spectroscopic studies of background H II regions or quasars probe relatively few points in a foreground disk, which induces a bias toward low absorption); (5) there is no need to correct for the internal extinction of the background galaxy or the Milky Way (as required in some spectroscopic studies of background objects shining through foreground disks); (6) our differential technique is not affected by color gradients due to stellar population gradients (provided they are symmetric), which complicates the use of color maps ($V-K$, $B-K$, etc.) as dust detectors (Block et al. 1994); (7) we do not need to make assumptions about the vertical structure of the disk or the relative z-distributions of stars and dust (these assumptions are needed when the disk's own light is used to probe extinction; see Elmegreen 1980); using the nonoverlapping parts of the galaxies, we can test directly for the requisite symmetry in azimuthal profiles; and (8) scattering corrections are also differential, which can keep them slight.

This technique also has some disadvantages relative to others: (1) there are rather few tractable objects nearby enough for spatially well-resolved analysis and (2) the success of the technique hinges on the degree of symmetry in both the foreground and background galaxies.

The extinction values we derive differ in a significant way from those derived from internal galaxy properties. Any technique relying on a galaxy's own radiation measures the dust content weighted by the distribution of starlight and dust in the galaxy itself. In our extinction measures, the light source (the background galaxy) is external to the opacity source (the foreground galaxy); thus, our extinction values are directly relevant, for example, to calculations of the cumulative effect of spiral disks on optical quasar counts. However, these measures may not be the most appropriate ones for calculating Tully-Fisher corrections, depending on the relative distributions of stars and dust.

It is useful to distinguish several regimes of galaxy backlighting, depending on the apparent sizes of the galaxies and the impact parameter of the background light. Quasars and distant galaxies projected behind other galaxies represent a limiting case in which the background sources are much smaller than foreground galaxies. These can provide reasonable extinction measures, particularly since scattering into the beam is negligible, but we may miss such small background objects if they are heavily absorbed by the foreground galaxies; that is, the use of such small probes is biased toward the clearest lines of sight (e.g., Disney 1995). Partially overlapping galaxies with similar angular size are not vulnerable to this particular selection effect; even extensive absorbing disks, almost opaque and larger than the luminous disk, would be detected in such pairs. Completely overlapping galaxies (e.g., NGC 3314; Keel 1983) are good for probing the central regions of disks, but with no nonoverlapping parts to provide estimates of the intrinsic disk brightness, the results are necessarily limited in accuracy. Finally, a spiral seen nearly edge-on may have its own disk backlit by its outer bulge (see van Houten 1961; Simien, Morenas, & Valentijn 1993; Knapen et al. 1995). These cases have very well understood geometry, but scattering effects can be much more important than in overlapping galaxy pairs (but were neglected in these studies). We will present our results on such "peeking bulges" in a later paper.

2.3. *Corrections for Scattering Effects*

We estimate the possible role of scattered light in our measurements, with scattering acting to "fill in" extinction (Witt et al. 1992). Scattering is potentially important because the bright central regions of a background galaxy may be close enough to the foreground galaxy for substantial amounts of light to be scattered into our line of sight by dust in the overlap regions. Our technique automatically subtracts off internally scattered light in the foreground galaxy, to the extent that it is as symmetrically distributed as the galaxy itself. Our procedure is sensitive only to scat-

TABLE 1

CANDIDATE OVERLAPPING GALAXY PAIRS

Pair	Observatory	Notes	Pair	Observatory	Notes
AM 0247−312	CTIO	S0+E	NGC 450	CTIO	This paper
AM 0313−545	CTIO	Interfering star	NGC 1531	CTIO	Tidal arm overlap
AM 0327−285	CTIO	S behind	NGC 1738/9	CTIO	This paper
AM 0500−620	CTIO	This paper	NGC 2207	KPNO	Possible
AM 0546−253	CTIO	Two SBs	NGC 3314	CTIO	This paper
AM 0645−264	CTIO	Tidal dist.	NGC 4567/8	Lowell	This paper
AM 1311−455	CTIO	This paper	NGC 4647/9	KPNO	This paper
AM 1316−241	KPNO	This paper	NGC 5090/1	CTIO	Asymmetric S
AM 2030−303	CTIO	Irr. structure	NGC 5544/5	Lowell	Possible
AM 2131−572	CTIO	Interfering star	NGC 6050	KPNO	Possible
AM 2344−282	CTIO	Pair 1: too small?	NGC 7016	CTIO	Possible
AM 2344−282	CTIO	Pair 2: too small?	NGC 7119	CTIO	Interfering star
AM 2347−292	CTIO	Too small?	NGC 7174	CTIO	Tidal dist.
AM 2354−304	CTIO	SBb+Sb	NGC 7284/5	CTIO	E in background
Anon 2345−29	CTIO	S+S, faint	NGC 7433	CTIO	Possible
Arp 40	KPNO	Possible	UGC 2942/3	CTIO	This paper
ESO 0245−53	CTIO	Possible	UGC 3445	Lowell	Too distorted
ESO 0320−51	CTIO	This paper	UGC 3995	Lowell	Possible
ESO 0416−50	CTIO	Possible	UGC 4619	Lowell	Possible
ESO 0433−41	CTIO	Inclined S+S	UGC 7535	CTIO	Possible
HCG 5	CFHT	From P. Hickson	UGC 8813	Lowell	S0+S0
IC 4378	CTIO	Possible	UGC 8972	KPNO	Possible
IC 4721	CTIO	Possible	UGC 9554	CTIO	Possible
IC 5328	CTIO	E+S0	UGC 10049	KPNO	Possible
IC 5349	CTIO	S0+compact	UGC 10422	Lowell	Possible
IC 5364	CTIO	Possible	UGC 11168	KPNO	Too detached
MCG 2-58-11	CTIO	Late-type S+S	Zh 0016−61	CTIO	Possible
NGC 45	CTIO	Small background group	Zh 2222−31	CTIO	Possible

tered light from the background galaxy. Furthermore, because we remove the symmetric counterpart of the foreground galaxy from the overlap region, we are also removing some background scattered light. Thus, we are affected only by *differential* scattering between the overlap region of interest and its symmetric foreground counterpart. This differential scattered light drops very rapidly for increasing separation of the galaxies along the line of sight. Further details of our scattering corrections can be found in the Appendix.

3. SAMPLE SELECTION

Suitable partially overlapping galaxy pairs are rare; were it not for gravity causing the galaxy covariance function to be much greater than unity at small separations, we would expect virtually no useful nearby candidates. We attempted to find all overlapping galaxy pairs among galaxies bright enough and large enough (in angular size) for absorption measures. We examined candidate pairs on Sky Survey images and obtained CCD images of the most promising.

Our observing sample is drawn from a variety of sources: we performed numerical searches for overlapping neighbors in the Revised Shapley-Ames Catalog (Sandage & Tammann 1981), the ESO-Uppsala survey (Lauberts 1982), the Uppsala General Catalog (Nilson 1973), the Revised New General Catalog (Sulentic & Tifft 1973), the NGC 2000 catalog (Dreyer 1888; Sinnott 1988), the Morphological Catalog of Galaxies (Vorontsov-Velyaminov & Krasnogorskaya 1962; Vorontsov-Velyaminov & Arkhipova 1963, 1964, 1968, 1974), the Karachentsev (1972) catalog of northern galaxy pairs, the Chinese catalog of double galaxies (Zhenlong et al. 1989), and the Third Reference Catalogue of Bright Galaxies (de Vaucouleurs et al. 1991). We selected all pairs with center-to-center separations of less than 1.5 times the sum of their cataloged isophotal radii R_{25}, if such size information was present. We also selected individual catalog entries in the UGC, ESO-Uppsala, and NGC listings that were typed as inherently multiple systems. We also visually inspected all pairs in the Arp-Madore (1987) catalog (including all objects with notes mentioning dust or absorption), the Arp (1966) Atlas of Peculiar Galaxies, and the Reduzzi & Rampazzo (1995) catalog of southern pairs. Further objects were drawn from visual inspection of the SRC J survey films in the Shapley supercluster region. Serendipity (while inspecting brighter candidates selected as above) and anecdotal lore provided a few more prospects, as well. Throughout these searches, we were especially alert for any objects with clear signs of absorption, and we certainly would have selected any galaxies with extensive absorption appearing beyond the optical disk as "bites" in background systems.

4. OBSERVATIONS

Promising overlapping candidates were observed using CCD cameras at Kitt Peak, Cerro Tololo, and Lowell Observatory. We have so far imaged 56 galaxy pairs, of which a dozen are tractable enough for detailed analysis. An additional dozen may admit more limited analysis. We have also observed several "peeking bulge" galaxies: nearly edge-on spiral galaxies whose bulges can be seen on either side of their disks, thus providing backlighting for the intervening disks; such individual systems can be analyzed in a similar, but not identical, fashion as the overlapping pairs. We concentrated on imaging in the B and I bands to give

the quickest route to measures over a long color baseline without risk of emission-line contamination. We rejected the U band for most objects since the gain in wavelength baseline and the effective extinction curve coverage are normally offset by losses as a result of fainter background light from early-type galaxies, lower chip efficiency, and increased Poisson noise at a given flux level.

Most of our targets were observed with the 1.5 m telescope at Cerro Tololo, using a Texas Instruments CCD binned during readout to provide 400 × 400 pixels at 0.″54 pixel^{-1} (in 1992 November) or a Tektronix 2048^2 device giving 0.″24 pixel^{-1} (1995 July). Observations at the 1.1 m Hall Telescope of Lowell Observatory (in 1991 March) used a Texas Instruments 800 × 800 CCD and 2:1 focal reducer, covering a large field 9.4 arcmin square at 0.″708 pixel^{-1}. This was especially important for pairs of large angular size such as NGC 4567/8 in Virgo. At the 2.1 m telescope of Kitt Peak National Observatory (1991 June), we used either the 1024^2 Tektronix CCD at 0.″305 pixel^{-1} or a Space Telescope Imaging Spectrograph (STIS) 1024^2 chip at 0.″27 pixel^{-1} (with the detector switch necessitated by a temporary detachment of the Tektronix chip from the cooling finger within the Dewar).

Based on the CCD images, we rejected many candidate pairs for being too asymmetric, for having the wrong galaxy in front (such as AM 0327−285; de Mello et al. 1995), for having a foreground star in the crucial region, or for morphological reasons (foreground E and S0 galaxies show no measurable absorption: $A_B \leq 0.1$ mag). The complete list of candidates imaged to date with the CCDs is given in Table 1, with reasons for the rejection of those not analyzed.

5. ANALYSIS OF INDIVIDUAL OBJECTS

This paper reports the results for overlapping pairs that we have found to be most tractable. Nonetheless, each system warrants individual discussion about the symmetry assumed or the particular limitations suggested by its structure or geometry. For the overlapping pairs analyzed in this work, their identifications, morphologies, velocities, isophotal radii, and axial ratios are given in Table 2. In the following discussion of individual objects, we will tend to quote magnitudes of extinction A rather than optical depths τ, where $A = 1.086\tau$. Typical errors in individual measurements are $\approx$0.15 mag (individual values are given in Table 3) and include photon statistics and systematic errors estimated from regions adjacent to or symmetric with the regions of interest. The objects are discussed in roughly descending order of quality, but their results are tabulated in alphabetical order.

5.1. *AM 1316−241*

As reported in White & Keel (1992), our best case thus far is AM 1316−241, an Arp-Madore catalog object consisting of a foreground Sbc projected against a background elliptical. Figure 2*a* shows the B-band image of this pair, which is also interesting because the recession velocity of the foreground spiral (10,365 km s^{-1}) is 660 km s^{-1} *larger* than that of the background elliptical (the single velocity listed in the ESO-LV catalog is attributed to the wrong pair member). As indicated in Table 2, the axial ratio of the foreground spiral is 4.42, implying an inclination of 77°.

Figure 2*b* shows a $B-I$ image, where the foreground overlapping spiral arm very obviously reddens the light from the background elliptical. The symmetry of each of the galaxies is good enough that we can employ the image cut-and-paste technique described in § 2 to estimate the opacity over a relatively large fraction of the overlap region. Figures 2*c* and 2*d* show the resulting maps of $e^{-\tau'}$ in the B and I bands, displayed with the same absolute intensity scale, the darker regions being more opaque. The opacity is clearly concentrated in the spiral arm, while the interarm region is nearly transparent. It is also obvious from Figures 2*c* and 2*d* that the arm is optically thicker in B than in I. Table 3 lists the face-on–corrected extinction in the arm and interarm regions, as well as for an average over the disk area seen in the $e^{-\tau'}$ maps of Figures 2*c* and 2*d*. In the ideal case of infinitely thin dust disks, the face-on–corrected extinctions are found by dividing the apparent extinction by the

TABLE 2

OVERLAPPING GALAXY PAIR PROPERTIES

	FOREGROUND PROPERTIES					BACKGROUND PROPERTIES	
FOREGROUND (Alternate Name)	Type	cz (km s^{-1})	R_{25}^B (arcsec)	Axial Ratio	BACKGROUND (Alternate Name)	Type	cz (km s^{-1})
AM 0500−620 (ESO-LV 1190270).....	Sbc	8420	28	1.49	ESO-LV 1190271	E	9200
AM 1311−455	Sa	3091	60.0	1.27	...	Sc	3110
AM 1316−241 (ESO-LV 5080451).....	Sbc	9554	37.5	4.42	ESO-LV 5080450	E	4317
ESO 032012−5150.1 (Fairall 299)	Sa	17328	22.5	1.11	...	S0	...
NGC 450 (UGC 806).....	S	2118	92.7	1.31	UGC 807	S	11431
NGC 1739	Sbc	3892	42.0	1.95	NGC 1738	Sbc	3978
NGC 3314a	S	2872	46.5	1.22	NGC 3314b	S	4426
NGC 4568 (UGC 7776)	Sbc	2255	137.0	2.29	NGC 4567 (UGC 7777)	Sbc	2274
NGC 4647 (UGC 7896)	S	1422	86.5	1.40	NGC 4649 (UGC 7898/M60)	E	1413
NGC 5545	Sbc	3302	37.8	2.86	NGC 5544	SB0/a	3292
UGC 2942	S	6361	39.5	3.70	UGC 2943	S	6434

TABLE 3

FACE-ON EXTINCTIONS

	ARM			INTERARM			AVERAGE		
GALAXY	R/R_{25}^B	A_B	A_I	R/R_{25}^B	A_B	A_I	R/R_{25}^B	A_B	A_I
AM 0500−620.....	0.6	$>2^{\pm 0.1}$	$1.4^{\pm 0.1}$	0.5	0.07–0.4	0.0–0.5	...	...	...
AM 1311−455.....	1.18	$0.78^{\pm 0.12}$	$0.24^{\pm 0.09}$	0.95	$0.24^{\pm 0.14}$	$0.08^{\pm 0.12}$	...	...	...
AM 1316−241.....	0.75	$0.39^{\pm 0.12}$	$0.15^{\pm 0.01}$	0.4–0.7	$0.09^{\pm 0.03}$	$0.05^{\pm 0.01}$	0.4–0.85	$0.21^{\pm 0.06}$	$0.14^{\pm 0.01}$
ESO 0320−51	...	...	...	0.44	$0.31^{\pm 0.18}$	$0.08^{\pm 0.08}$	...	...	...
NGC 450	...	...	...	0.95–1.0	<0.08	<0.08	...	...	...
NGC 1739.....	0.65	0.30–0.37	0.24–0.28	0.55	0.20–0.26	$0.17^{\pm 0.04}$	...	...	...
NGC 3314.....	0.16	$1.31^{\pm 0.18}$	$1.02^{\pm 0.20}$	0.19	$0.91^{\pm 0.14}$	$1.31^{\pm 0.04}$	...	...	...
...	0.34	$1.34^{\pm 0.09}$	$0.67^{\pm 0.15}$	0.28	$0.63^{\pm 0.24}$	$0.48^{\pm 0.26}$	...	...	...
...	0.42	$0.91^{\pm 0.09}$	$0.67^{\pm 0.15}$	0.39	$1.43^{\pm 0.17}$	$0.52^{\pm 0.20}$	...	...	...
NGC 4568.....	0.5–0.85	$1.20_{>0.44}$	$0.69^{+0.79}_{-0.28}$	...	...	...	...	...	...
NGC 4647.....	≥1	<0.11?	<0.11?	...	...	...	...	...	...
NGC 5545.....	0.77	$0.45^{\pm 0.03}$	$0.35^{\pm 0.02}$	0.77	$0.18^{\pm 0.05}$	$0.10^{\pm 0.03}$	...	...	...
UGC 2942.....	...	...	...	...	...	...	0.56	$>0.40^{\pm 0.07}$	$0.36^{\pm 0.04}$

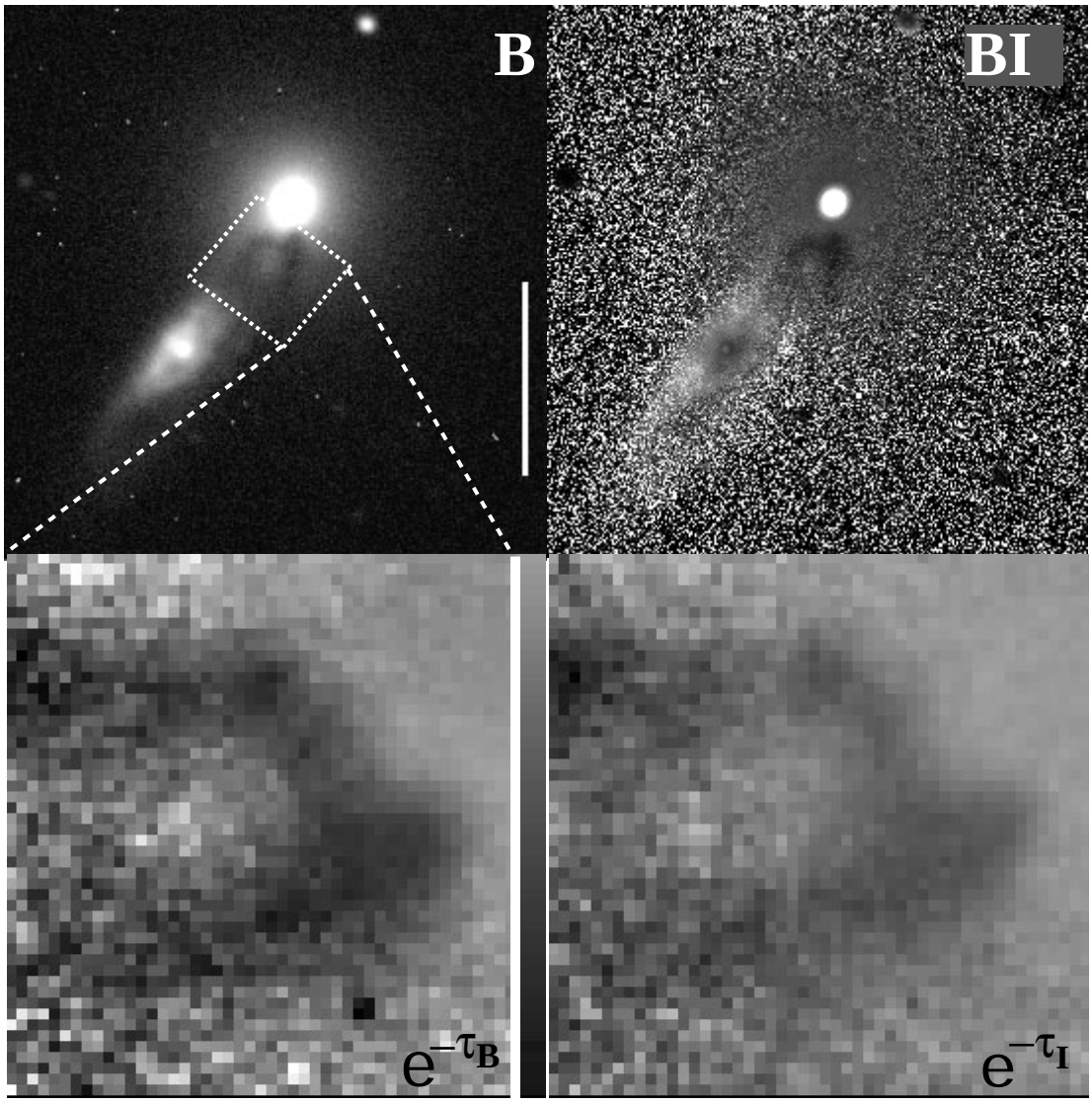

FIG. 2.—AM 1316−241: the foreground galaxy is the large inclined spiral to the southeast. The scale bar is 30″ for all of the images except Fig. 13. North is at the top and east to the left for all of the B and $B-I$ images. (*a*) B-band image, indicating area blown up for opacity maps in lower panel; (*b*) $B-I$ color image; (*c*) $e^{-\tau_B}$; (*d*) $e^{-\tau_I}$, with the $e^{-\tau}$ images rotated to align with the spiral's major axis. Both galaxies in this pair are symmetric enough to allow the detailed decomposition illustrated in Fig. 1. The strong absorption is concentrated into the projected spiral arm, with much less in the interarm region just inside it. The opacity maps are displayed at the same brightness scale, showing how much smaller the extinction is at I compared to B.

galaxy's axial ratio; this correction will be an overestimate for the more realistic cases of finite thickness and clumped absorbers. The resulting extinctions are rather small: in the blue, $A_B = 0.39$ in the arm region and 0.09 in the interarm region, while in I, $A_I = 0.15$ and 0.05 in the arm and interarm regions, respectively. The arm is at 0.75 R^B_{25} (where R^B_{25} is the radius at which the blue surface brightness $\mu_B = 25$ mag arcsec^{-2}; see Table 2), while the measurable disk region extends from 0.37 to 0.85 R^B_{25}. The radial extents of these various regions are also given in Table 3.

5.2. *AM 0500−620*

The E/Sbc pair AM 0500−620 shares some of the favorable characteristics of AM 1316−241: it is comprised of a relatively undisturbed foreground spiral and a symmetric background elliptical (see Fig. 3*a* for a *B*-band image). In this pair as well, the elliptical can be accurately modeled from its unobscured half, and the spiral is symmetric enough for rotational symmetry to match its structure in some detail. In practice, each galaxy was modeled and subtracted from the data iteratively to converge on good models for each component separately. The absorption follows the arm as traced in $B-I$ quite closely (see Fig. 3*b*). After correcting for inclination ($a/b = 1.49$), we find face-on values of $A_B > 2$ and $A_I = 1.4$ along the arm ridge line, while the interarm extinction ranges over $A_B = 0.07$–0.4 and $A_I = 0$–0.5 at various points seen against the elliptical (see Table 3). The symmetry of this system is good enough to allow the construction of $e^{-\tau}$ maps, as for AM 1316−241 above. Figures 3*c* and 3*d* show maps of $e^{-\tau_B}$ and $e^{-\tau_I}$, respectively, with the same residual intensity scaling.

5.3. *NGC 1738/9*

Figures 4*a* and 4*b* are *B* and $B-I$ images, respectively, of the Sbc pair NGC 1738/9. The symmetry of this system is not good enough to do an opacity analysis in the same detail as for AM 1316−241 and AM 0500−620. Instead, the two regions indicated in Figure 4*a* are investigated: a foreground arm region at 0.65 R^B_{25} and an interarm region at 0.55 R^B_{25}. Symmetric regions in the foreground and back-

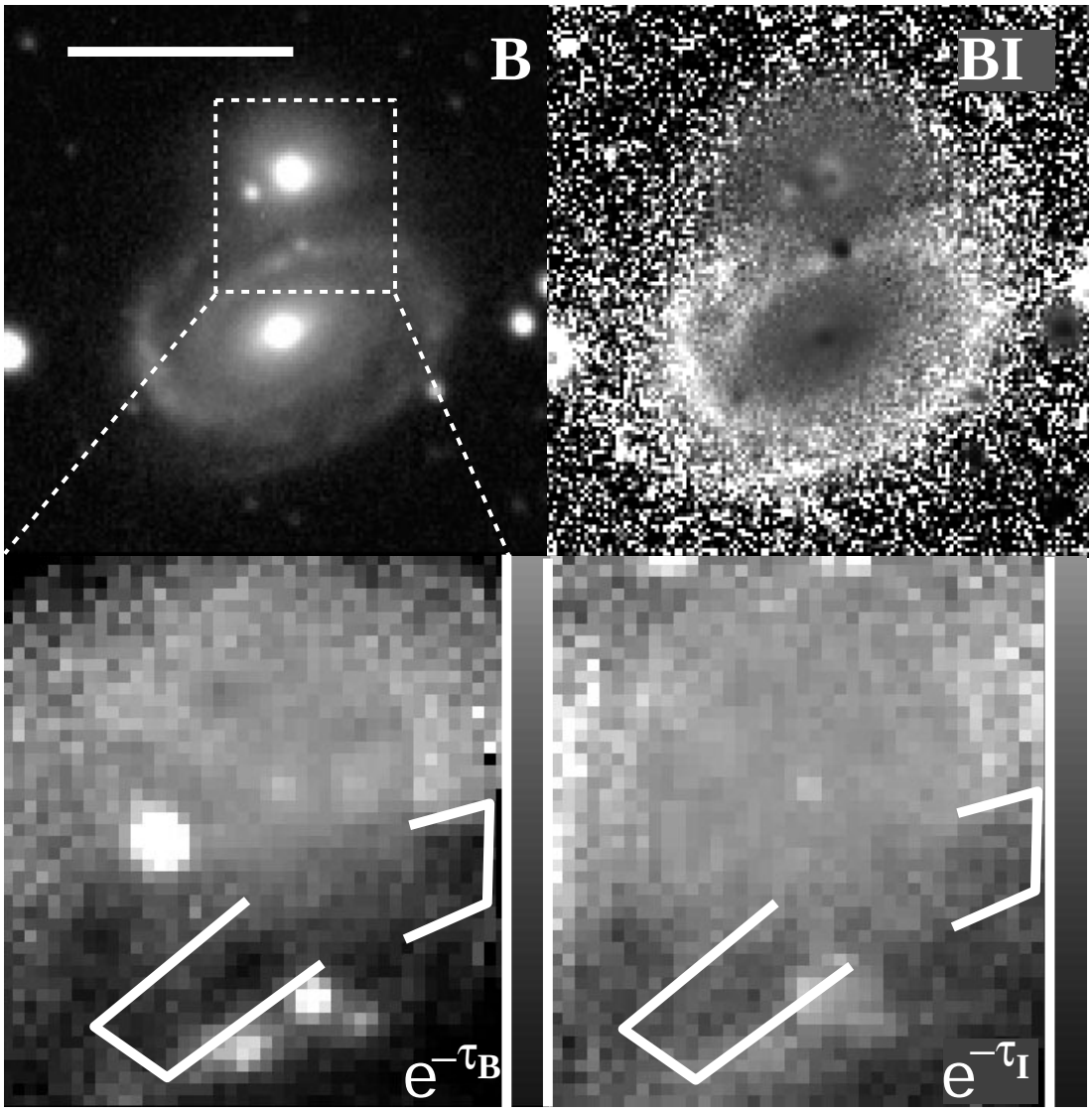

FIG. 3.—AM 0500−620: the foreground galaxy is the large spiral to the south. (*a*) *B*-band image, indicating area blown up for opacity maps in lower panel; (*b*) $B-I$ color image; (*c*) $e^{-\tau_B}$; (*d*) $e^{-\tau_I}$. The dust arm, indicated by the white brackets, crosses from the lower left corner to the right center edge. A very red foreground star appears just to the south of this arm, most apparent in the $B-I$ image. Again, the scaling for the opacity images is identical for *B* and *I*.

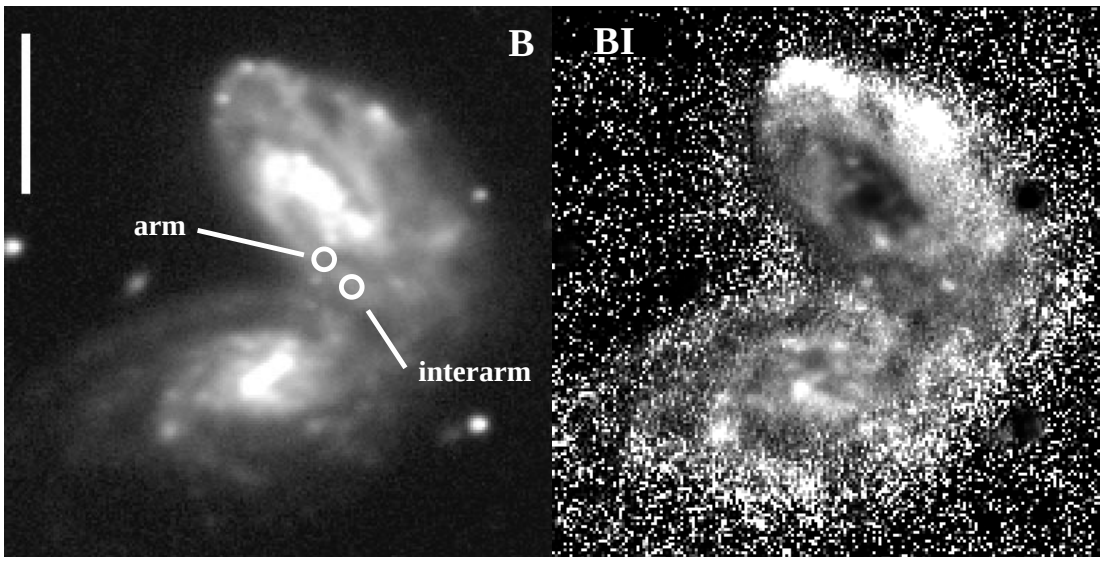

FIG. 4.—NGC 1738/9: the foreground galaxy is NGC 1739, the spiral to the south. (*a*) *B*-band image; (*b*) $B-I$ color image. In this pair of spirals, averages were taken over the marked regions, and symmetric areas (with regard for the spiral pattern) were used to estimate both foreground and background contributions.

ground galaxies are used to infer the apparent extinction in B and I in these two regions. The apparent extinction values of the foreground galaxy (NGC 1739) are divided by its axial ratio of 1.95 (indicating an inclination of 59°) to give the face-on–corrected values listed in Table 3. The face-on extinctions are again quite low: in the arm region, $A_B = 0.3$–0.37 and $A_I = 0.24$–0.28, while in the interarm region, $A_B = 0.2$–0.26 and $A_I = 0.17$.

5.4. *NGC 4567/8*

The Sbc pair NGC 4567/8 (UGC 7777/6) is another case in which the analysis is limited by the general lack of symmetry (see Figs. 5*a* and 5*b* for B and $B-I$ images). Here we concentrate on the dark lane in the upper left of Figure 5*a* that cuts across a brighter background galaxy arm. The comparison region for the foreground arm is taken from a region along the arm but beyond the projected bulk of the background galaxy (farther to the upper left in Fig. 5*a*); the comparison region for the background arm is along the background arm, just away from where it is blocked by the foreground galaxy. The foreground galaxy (NGC 4568/UGC 7776) has an axial ratio of 2.29, implying an inclination of 64°. The assessed region in the foreground galaxy samples, in projection, a range of radii spanning 0.5–0.85 R^B_{25}. We calculate face-on extinctions of $A_B \sim 1.2$ and $A_I = 0.69$ for this region (see Table 3).

The interpretation of the light seen beyond the strong dust lane in NGC 4568 (to the lower left of the region analyzed above) as coming from the background galaxy rather than the foreground structure hinges on whether any similarly bright areas are found at comparable projected radius in NGC 4568 and on the rather symmetric shape of NGC 4567 as seen in the less obscured I band. Inspection of archival *Hubble Space Telescope* (*HST*) "snapshot" images obtained in the F606W filter (WFPC2 data sets U29R4H01/2; PI G. Illingworth) shows that most of the excess light in this area comes from distinct bright clusters and associations, brighter than any others seen in the foreground object at comparable radius but quite comparable to the (systematically brighter) star-forming regions in the background system (see Fig. 5*c*). This somewhat strengthens our interpretation of the excess light as indeed shining through a more transparent interarm medium.

The WFPC2 data also show that the darkest absorbing clouds in this pair, with a measured extinction of $A_{606} \approx 1.5$, are two irregular resolved features about 7″ (0.5 kpc) in extent but narrow enough (<1″) that they are not prominent in our ground-based images. Both are located well beyond the spiral arms (and other dust features) in NGC 4568 (as marked in Fig. 5*c*). Their low residual intensity requires that they be in the foreground, not part of NGC 4567 in the background. Either they are isolated in the outer disk or are located several kiloparsecs from the disk plane (either of which might be attributed to the effects of interactions between these two galaxies). We cannot immediately exclude the possibility that they are in the extreme foreground of the Milky Way itself, though the surface density of such clouds could not be very large without violating constraints from the number *not* seen in *HST* imagery of elliptical galaxies and the intensity of high-latitude IR cirrus emission.

5.5. *UGC 2942/3*

This is a pair of highly inclined spirals, with the background galaxy seen only a few degrees from edge-on (Figs. 6*a* and 6*b* show B and $B-I$ images). The dust lane in the background galaxy provides a recognizable target to seek through the foreground disk. For cases like this, scattering corrections become unnecessary since the edge of the background dust lane is a sharp target; even small-angle scattering would contribute only over a larger angular scale.

To estimate the extinction in the foreground spiral UGC 2942, we consider intensity slices perpendicular to the projected plane of the background galaxy UGC 2943. These are taken in the overlap region and at the corresponding locations on the opposite side of UGC 2943. As shown in Figure 6*c*, both B and I profiles show a feature corresponding closely to the position and form of the background galaxy, dimmed by factors of order <0.26 in B and 0.29 in I. The B value is particularly uncertain as a result of fore-

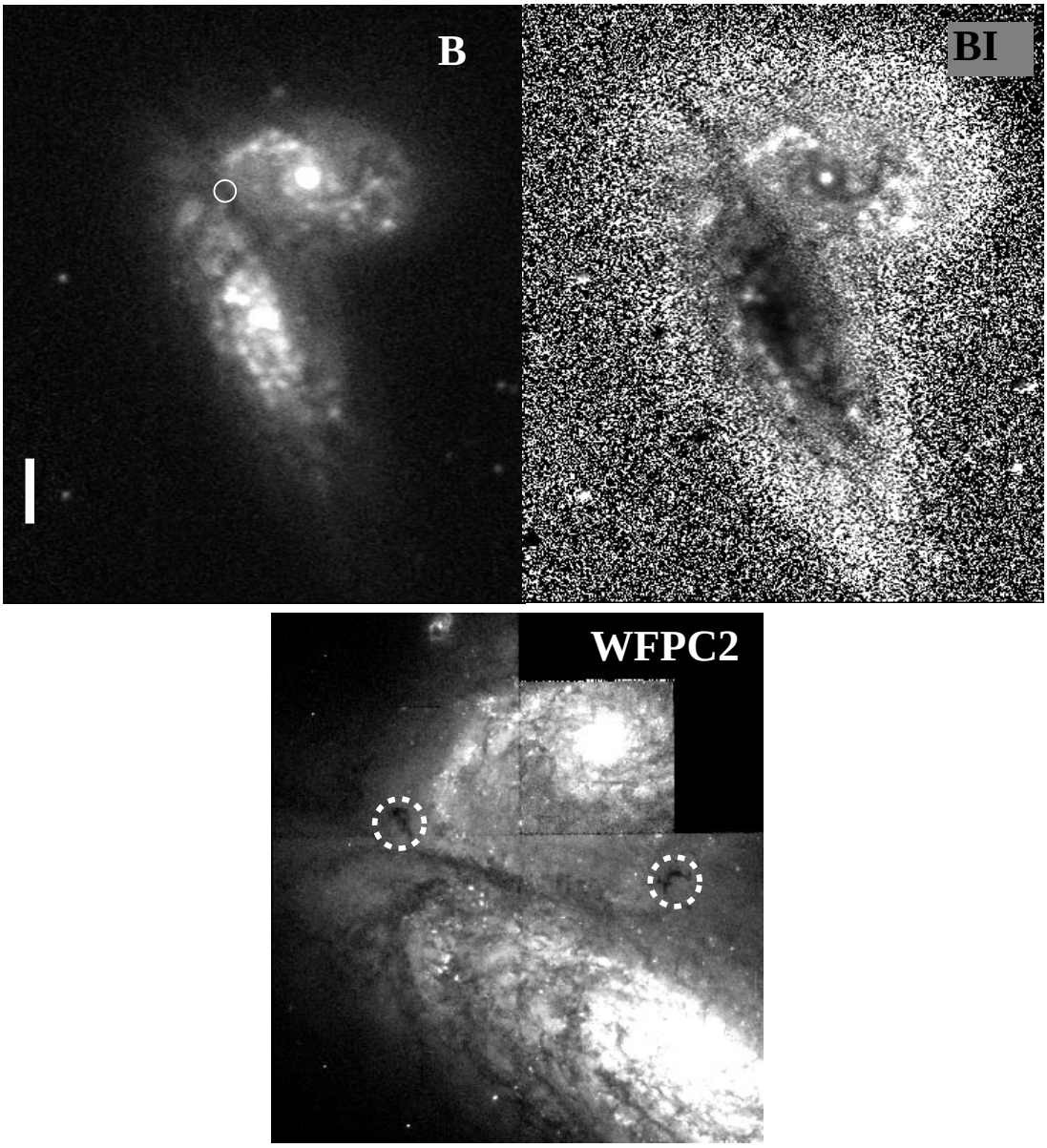

FIG. 5.—NGC 4567/8: the foreground galaxy is NGC 4568, the spiral to the south. (*a*) *B*-band image; (*b*) $B-I$ color image; (*c*) mosaic of WFPC2 F606W images, rotated to the nearest quadrant from cardinal orientation. The *HST* imagery shows the brightest associations used to attribute light past the dusty arm of NGC 4568 to the background arm of NGC 4567. This mosaic also shows several narrow dust clouds of high optical depth beyond the main disk of NGC 4568 (*within the dashed circles*). They are sufficiently smeared by seeing to be inconspicuous in the Lowell image above.

ground structure, but even this detection is significant above the 3 σ level. We can exclude the possibility that the ratio of *B* and *I* extinctions follows a Galactic reddening law, which most likely means that the extinction is dominated by a few regions of large optical depth rather than widely spread extinction. Some such structure is visible in UGC 2942, especially in the *I* image (Fig. 6*c*). A foreground dust lane crosses the northern part of the overlap region, and in fact the signature of background light is detected only south of this region. The implied optical depth across the spiral arm (within the dust lane) is at least $\tau_B > 1.3$. The axial ratio of the foreground galaxy is 3.7, so the face-on–corrected extinctions are $A_B > 0.40$ and $A_I = 0.36$.

Both galaxies in this pair have reasonably widespread line emission, so that measurement of a Balmer decrement from H II regions in the background galaxy might give independent extinction measures for at least those lines of sight where we detect background regions (as was done for NGC 3314 by James & Puxley 1993). We attempted such a measurement for UGC 2942/3 using spectra obtained with the KPNO 2.1 m telescope and GoldCam spectrometer, along the major axes of each galaxy. Accurate emission-line rotation curves were measured (Fig. 6*d*), but the galaxies have orientations and rotation directions that defeat this technique; their rotation directions make the redshifts observed in the overlap region match to within a few tens of kilometers per second.

5.6. *AM 1311−455*

AM 1311−455 is comprised of a foreground ringed Sa projected against a rather disturbed Sc/d galaxy. Dust in the resonance ring is clearly seen to attenuate light from the background galaxy in the *B* image of Figure 7*a*. Structure in the background galaxy is evident through the regions inside

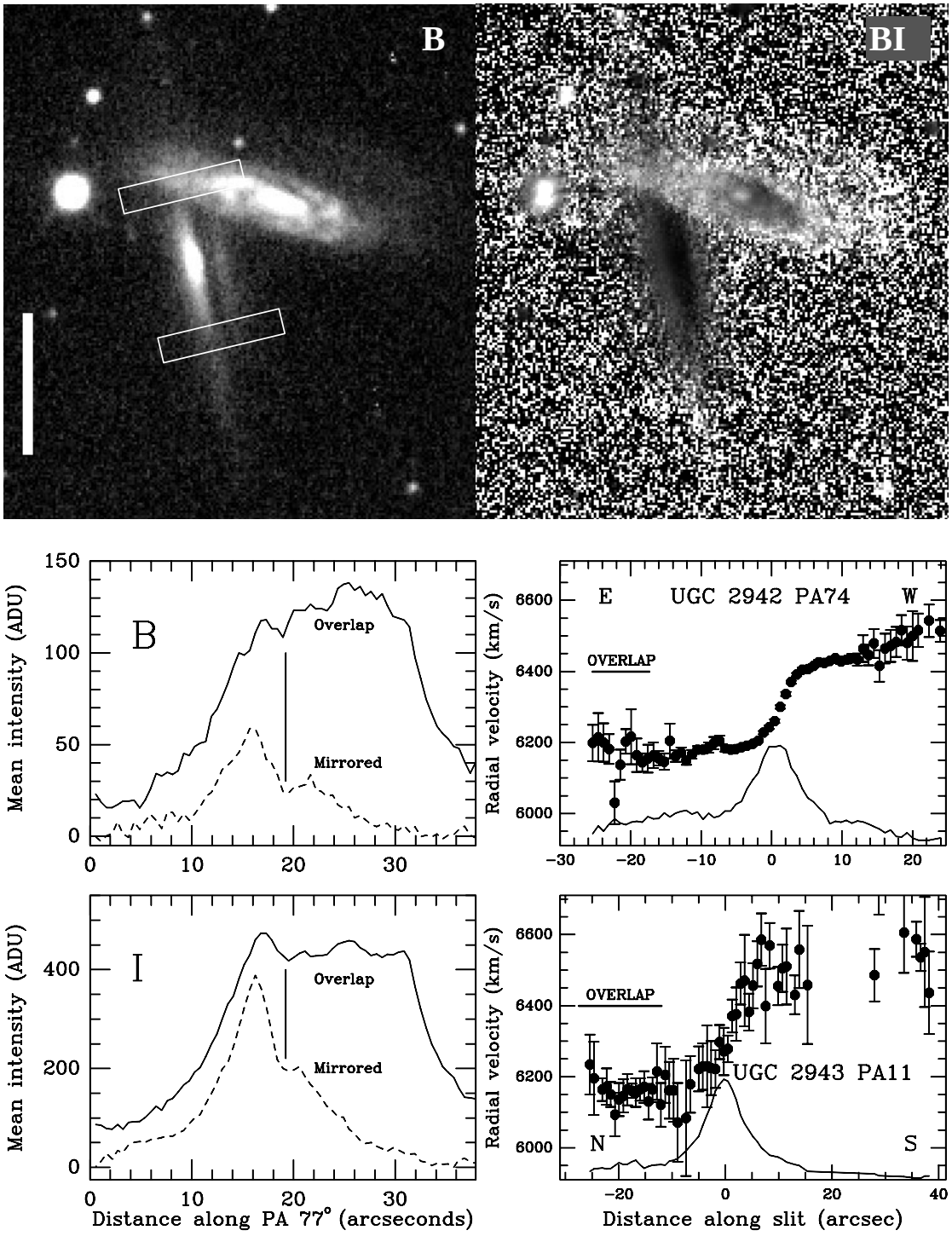

FIG. 6.—UGC 2942/3: the foreground galaxy is UGC 2942, the spiral to the north. (*a*) *B*-band image, logarithmically scaled; the white rectangles show the areas averaged for the intensity strips compared in (*c*). (*b*) $B-I$ color-ratio image. (*c*) (*left two panels*) Intensity slices parallel to the minor axis of UGC 2943, crossing the overlap (*solid line*) and symmetric (*mirrored*, *dashed line*) locations. The vertical bar indicates the deepest part of the dust lane in the background system UGC 2943, and the amount of extinction is measured from the relative intensity depth of this dip in the two slices at each passband. A region 10″ wide was averaged for each intensity trace. (*d*) (*right two panels*) Hα-[N II] emission-line rotation curves for UGC 2942/3. Error bars are $\pm 2\ \sigma$ from photon statistics, and the lower curves trace the red-light intensity along the slit. The near coincidence of radial velocity in the overlap regions defeated our attempt to use redshift separation to distinguish emission from the individual galaxies. Radial velocities are shown in the heliocentric frame; we derive nuclear redshifts of 6261 ± 5 km s^{-1} for UGC 2942 and 6269 ± 20 for UGC 2943.

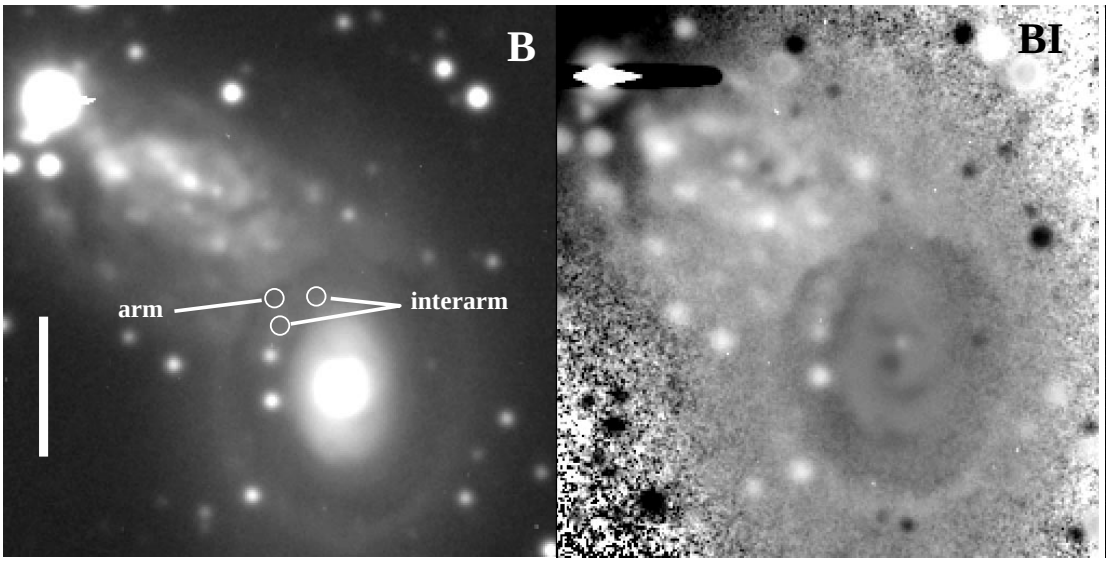

FIG. 7.—AM 1311−455: the foreground galaxy is to the southwest. (*a*) *B*-band image; (*b*) $B-I$ color image. In the color-ratio image, differences in seeing between the *B* and *I* data have been largely compensated by smoothing the *I* image with the best-matching Gaussian. Note that features in the arms of the background Sc system can be traced across the resonance ring in the SBa foreground galaxy, confirming low extinction immediately within the resonance ring.

and outside the ring. The resonance ring appears reddened in the $B-I$ color image of Figure 7*b*. In the ring itself (at $1.18R_{25}$) we find face-on–corrected ($a/b = 1.27$) values of $A_B \approx 0.78$ and $A_I = 0.24$. We also analyzed regions to the interior of the ring, at $0.95R_{25}$, and find the disk to be nearly transparent: $A_B \approx 0.24$ and $A_I \approx 0.08$.

5.7. *ESO 0320−51*

ESO 0320−51 is a foreground, face-on ringed galaxy projected against an edge-on S0 (see Figures 8*a* and 8*b* for *B* and $B-I$ images). The ring galaxy is likely to have recently had a collision with the small galaxy seen projected just within the western edge of the ring. The *B* image and the color-ratio map show a slight discontinuity where the ring crosses the S0, which suggests that the S0 is in the background. Comparison of *B* and *I* images shows that the ring obscures the edge-on disk more in *B* than in *I*, which more strongly indicates that the S0 is in the background. Detailed differential analysis confirms this, given that a small amount of extinction is found in *B* in the interarm region (at $0.44R_{25}$): $A_B = 0.31$ (face-on corrected, with $a/b = 1.11$); our measured *I* extinction in the same region is small but poorly determined since it is comparable to its error: $A_I \approx 0.08$. We were not able to derive an accurate extinction measure in the ring itself because of the patchy distribution of Hα-emitting knots at the intersection of the ring with the background S0 (Chatzichristou 2000).

5.8. *NGC 3314*

NGC 3314, a remarkable superposition of two spirals in the Hydra Cluster (Abell 1060), was considered in the context of opacity measurements by Keel (1983). Our more

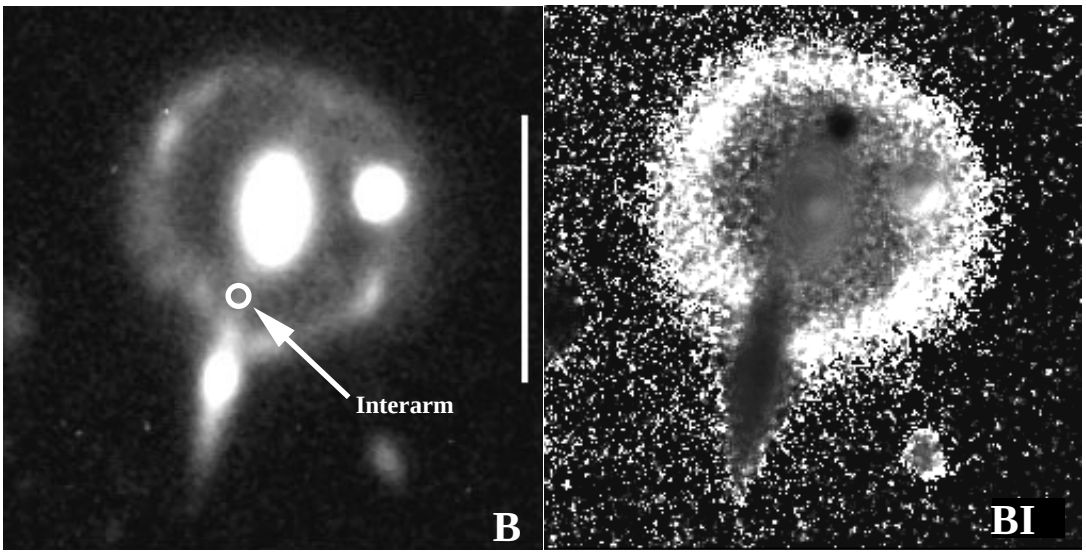

FIG. 8.—ESO 0320−51: the foreground galaxy is to the north; (*a*) *B*-band image; (*b*) $B-I$ color image. The combination of color and intensity data indicate that the edge-on galaxy is in the background, thus probing the ring and disk of the foreground, face-on system.

recent imaging allows us to greatly improve upon these measurements (B and $B-I$ images are shown in Figs. 9*a* and 9*b*). Following McMahon et al. (1992), we will call the foreground Sc galaxy NGC 3314a and the background Sab system NGC 3314b. Color-index maps, the symmetry of rotation curves (Schweizer & Thonnard 1985), and our K-band imagery show that the nuclei are separated by only 1.″8. We cannot do as complete an analysis here as for the best-case partial overlaps with a background E/S0 galaxy because (1) the background object is a spiral (albeit of early type) and (2) the overlap is so nearly central that there is no empirical check on the brightness profile of the background galaxy. However, this system is uniquely valuable because we can estimate extinctions in the foreground galaxy closer to its center than in any other sample member.

The best places for reliable extinction measurements are the points where the arms of NGC 3314a cross the disk edges of NGC 3314b, going from projection against the bright disk to projection against almost blank space at essentially the same radial distance for the arm. We measured the arm intensities at adjacent points on and off the background disk, after subtracting a minimal exponential-disk model to flatten most of the background gradient (so that interpolation to get the relevant unobscured background intensity is better constrained). For several locations where the arms cross the disk between 0.16 and $0.42R_{25}$, A_B ranges from 0.9 to 1.3 mag, while A_I ranges from 0.7 to 1 mag (face-on corrected, with $a/b = 1.22$). For interarm regions between 0.19 and $0.39R_{25}$, the (face-on–corrected) extinctions remain high: $A_B \approx 0.6$–1.4 and $A_I \approx 0.5$–1.3. The spiral pattern in NGC 3314a is defined more by the dust lanes than by the stellar distribution.

The H I maps presented by McMahon et al. (1992) afford a chance for a crude measurement of the dust-to-gas ratio, as represented by $N(\mathrm{H\ I})/E_{(B-V)}$, limited by the resolution of their VLA H I synthesis (FWHM about 14″), as compared to the arm width (traced by optical extinction) of about 5″ in the regions we have analyzed. Their Figures 3 and 4 suggest an H I column density of about 10^{21} cm^{-2}, and application of the usual Galactic extinction law to our values of A_B implies a ratio $N(\mathrm{H\ I})/E_{(B-V)} > 2.8 \times 10^{21}$ cm^{-2}; the upper limit is due to the likelihood that the H I is clumped into arms not well resolved in the H I map. Thus, we find a ratio of the same order as in our local neighborhood, and it is not clear how close a correspondence we should expect even for identical grain populations as a result of the effects of unresolved clumping on the spatially averaged extinction values we measure.

5.9. *NGC 5545/4*

NGC 5545/4 consists of an Sbc galaxy projected against an SB0/a galaxy. This pair was analyzed by Domingue et al. (1999), and the results are included for completeness in Table 3. Domingue et al. (1999) quote apparent extinctions, so we divided them by the axial ratio ($a/b = 2.86$) of NGC 5545 to produce face-on–corrected values.

5.10. *NGC 450/UGC 807*

This galaxy pair is comprised of NGC 450 (UGC 806), an Sc/Sd system at $cz = 1863$ km s^{-1}, and UGC 807, a spiral of earlier type at $cz = 11{,}587$ km s^{-1} (Figs. 10*a* and 10*b* show B and $B-I$ images). Rubin & Ford (1983) sought luminosity and distance indicators from rotation curves of this pair (with conclusions disputed by Moles et al. 1994). The large redshift difference effectively rules out the possibility of interaction, so that the line-of-sight distance is large and scattering effects can be ignored. We used two approaches to remove the foreground light from NGC 450. One parallels that used by Andredakis & van der Kruit (1992) for this pair, i.e., modeling the whole foreground galaxy with the STSDAS *ellipse* task, letting it average over small-scale structure, and subtracting the resulting smooth model. Since UGC 807 has a substantially smaller angular diameter than NGC 450, we could also make radial cuts adjacent to it and interpolate between them as a more local measure of foreground light. In neither case do we detect any extinction upon comparison of the "inner" and "outer" halves of UGC 807 in surface brightness or color, to limits of $\Delta(B-I) < 0.05$ and $A_B < 0.08$ (after dividing by

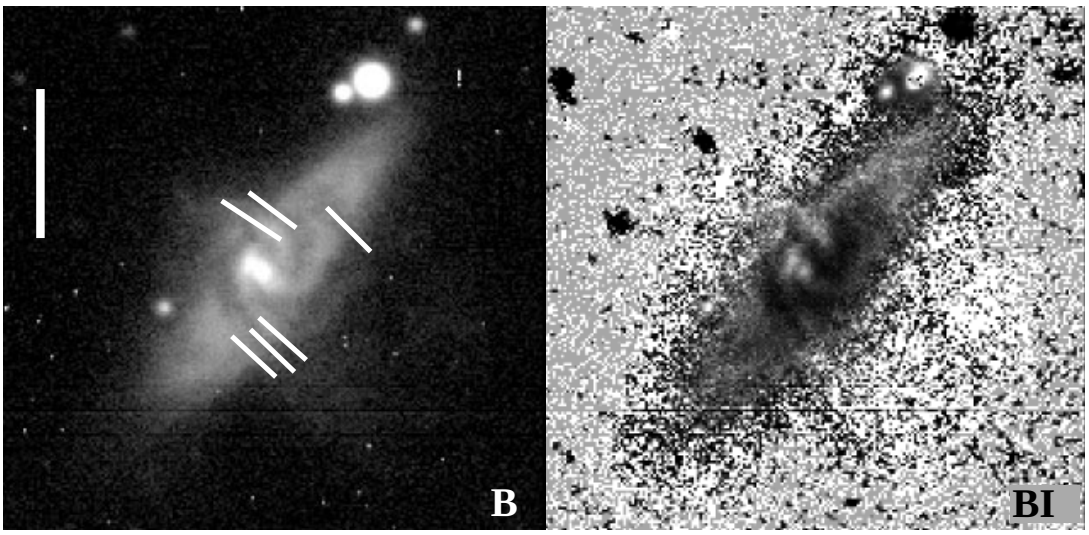

FIG. 9.—NGC 3314: the foreground galaxy is the more face-on spiral. (*a*) B-band image; (*b*) $B-I$ color image. Extinction measurements in this pair used slices along the foreground arms on and off the dust lanes, as indicated on the B image, and the amplitude of the disk edge from the background galaxy as transmitted, to yield opacity estimates. The superposition is almost perfect in this instance, with the nuclei separated by only 1.″8.

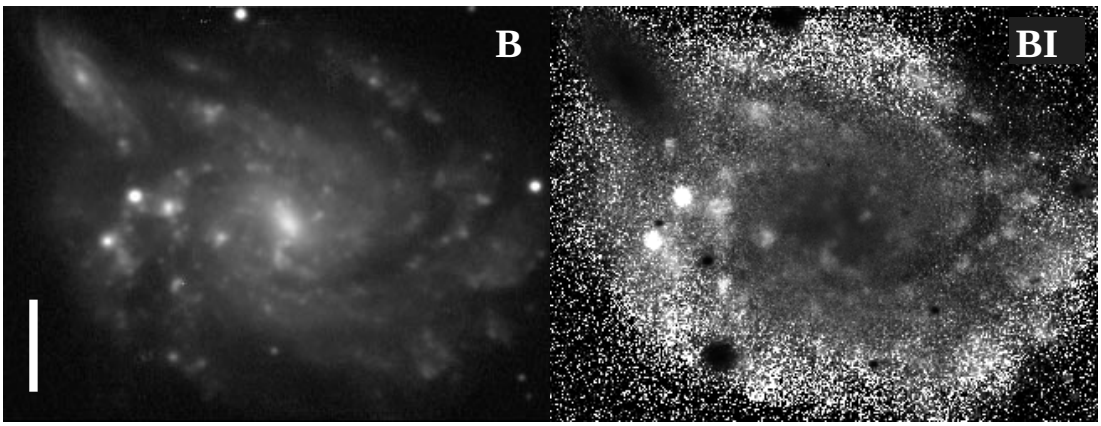

FIG. 10.—NGC 450/UGC 807: the foreground galaxy is the larger one to the southwest. (*a*) *B*-band image; (*b*) $B-I$ color image. No reddening or extinction was detected in this pair. The smaller galaxy UGC 807 has a redshift 6 times as great as NGC 450 and is thus clearly in the background.

a face-on correction factor of $a/b = 1.31$) across the outer disk edge. The measured area lies at about 0.95–1.0R_{25}.

5.11. *NGC 4647/9*

NGC 4647/9 is a bright, well-known pair in the Virgo Cluster (see the *B* band image in Fig. 11). NGC 4647 (UGC 7896) is a spiral with flocculent structure and heavy dust lanes, especially prominent at the edge of the optical disk (see, e.g., the photograph in Arp 1966, where this pair is number 116). They are projected at the large center-to-center separation of 11.9 kpc (for a distance of 16 Mpc) even compared to the large scale of the elliptical NGC 4649 (=M60=UGC 7898), so this pair offers a chance to examine primarily any dust structure that might lie beyond the bright optical disk (since the entire spiral is projected against detectable light from NGC 4649). The elliptical was modeled in two stages, using the STSDAS *ellipse* task for the inner parts of the galaxy and the best-fit global $r^{1/4}$ model beyond $r = 106''$, to avoid the spiral's influence on fitted isophotes. The outer regions are fitted by a somewhat shallower profile ($R_e = 82''$) than the global value of 68″ listed in the RC3 (de Vaucouleurs et al. 1991). After subtraction of this model for the elliptical component NGC 4649, no absorption structure is found beyond the edges of the disk of NGC 4647, with the outermost detected absorption associated with the prominent dust lane on the northern side of the disk. *If* the spiral is in fact in front, no dust features large enough to resolve have A_B or $A_I > 0.11$ (dividing by a face-on correction factor of $a/b = 1.4$). The range sampled here is at and outside R_{25}.

6. SUMMARY AND DISCUSSION

We have presented absolute extinction measures for 11 spiral galaxies in overlapping pairs. For each pair, there is some range of radii for which we can measure the residual intensity of background light transmitted through the foreground disk. We translate these measures into arm and interarm extinctions (where such a distinction is possible) in both *B* and *I* bands. In almost all cases, there is a large difference between arm and interarm values. In arm regions,

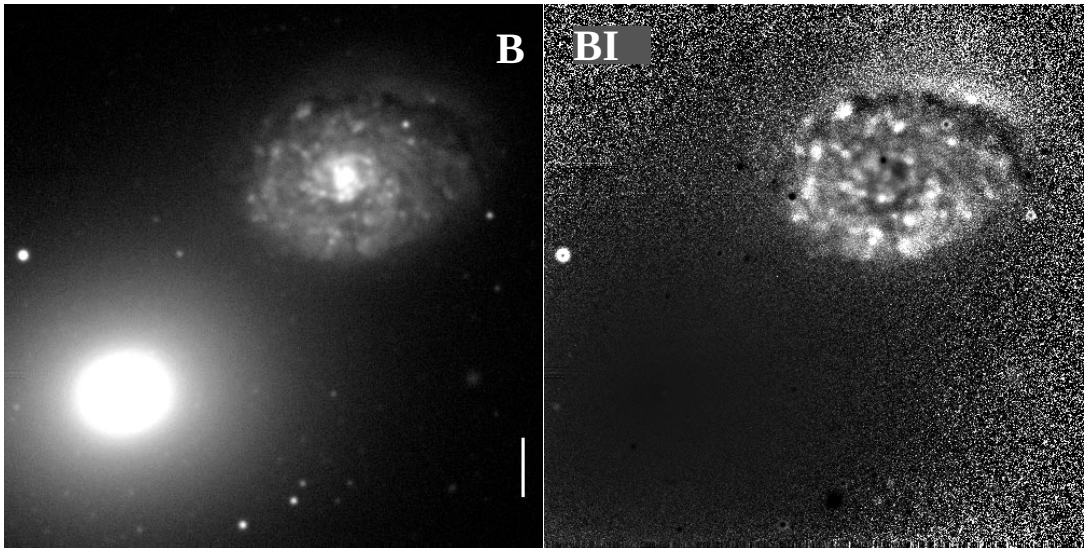

FIG. 11.—NGC 4647/9: we have no direct evidence of which galaxy is foreground. (*a*) *B*-band image; (*b*) $B-I$ color image. There remains ambiguity in this pair as to whether the spiral is in front or behind, since both are Virgo Cluster members and we detect no absorption outside the spiral disk against the extensive envelope of the elliptical NGC 4649.

$A_B \approx 0.3$–2 and $A_I \approx 0.15$–1.4, while in interarm regions, $A_B \approx 0.07$–1.4 and $A_I \approx 0.05$–1.3. Table 3 summarizes the pairs and regions for which extinction measurements have been made. The top panel of Figure 12 graphically summarizes these results for arm regions, while the bottom panel of Figure 12 does the same for interarm regions (solid and dotted diamonds represent values of A_B and A_I, respectively). The arm and interarm plots are drawn to the same scale to emphasize that arm regions tend to be much more opaque than interarm regions. Within each plot it is also clear that there is more extinction in B than in I, as expected.

The interarm ("disk") extinction tends to decline with radius (Fig. 12, *bottom panel*) from A_B values of only ~ 1 mag within $\sim 0.3R_{25}$. In contrast, spiral arms and resonance rings can be optically thick at almost any galactocentric radius. We do not see evidence for substantial extinction in the outer parts of disks (and such extinction would have been obvious even in our initial screening as "bites" taken out of background galaxies). The radial distribution of B and I extinction in interarm regions can be characterized by exponential scale lengths that are consistent with the exponential scale length h_* of stars in typical spiral disks: $h_* \approx 0.28R_{25}$ (Simien & de Vaucouleurs 1986). We thus find that the interarm dust has a scale length similar to that of the disk starlight, in agreement with the Kylafis & Bahcall (1987) result of near equality found from photometric decomposition of the edge-on spiral NGC 891. Presently known sites of grain formation (in particular, kinds of stellar atmospheres and expanding envelopes) naturally give rise to dust distributions that are tied to those of stars.

We find no correlation between extinction properties and galaxy Hubble type in our sample. However, most of the galaxies in our sample are type Sbc or a bit later; only two are as early as Sa (AM 1311−455 and ESO 032012−5150.1), and these have arm and interarm extinctions typical of the whole sample.

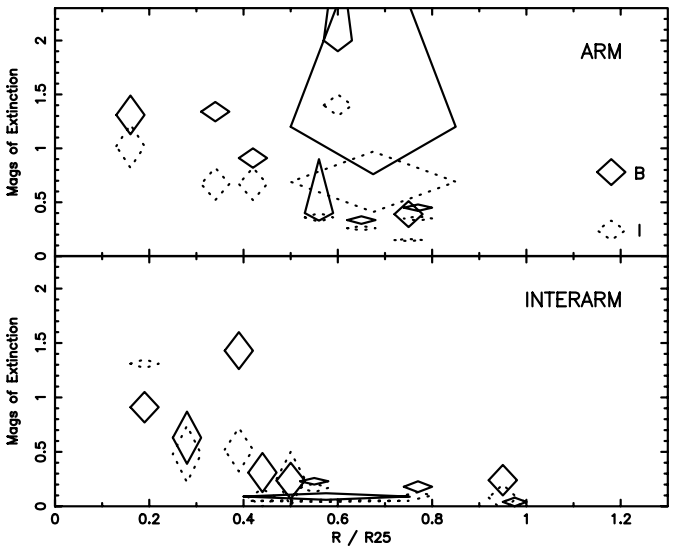

FIG. 12.—Summary of all face-on–corrected extinction measurements. *Top*: extinction magnitudes in arm regions as functions of R^B_{25}, with A_B (A_I) values indicated by solid (dotted) diamonds; *bottom*: extinction magnitudes in interarm regions as functions of R^B_{25}. The arm measurements show no obvious trend with galactocentric radius, but the interarm extinction drops with distance from the nucleus in a way that can be well described by an exponential in extinction (and thus in column density). The scale length of this form is close to that for the disk starlight in a typical spiral.

Our initial results on AM 1316−241 (White & Keel 1992) led us to conclude that disk opacity is concentrated in spiral arms and that interarm regions are fairly transparent. Our newer work is generally consistent with this picture, with resonance rings found to be as optically thick as spiral arms. Therefore, the distribution of absorption tends to be spatially correlated with particularly bright regions since spiral arms are brighter than interarm regions. We (White & Keel 1992) suggested that this spatial correlation between internal extinction and emission may account for the statistical results reported in earlier studies, i.e., that surface brightness is roughly independent of inclination. The dust is optimally placed to affect global blue photometric properties since typically half the disk light comes from only about 20% of its area, accounting for the rather flat inclination–surface brightness relation, *without* requiring galaxies to be optically thick in interarm regions. These remarks are directed particularly to grand-design spirals since in flocculent systems we cannot make a clear distinction between arm and interarm regions.

Closer examination of Table 3 shows that the relation between A_B and A_I is consistent in arm and interarm regions, given our errors; in other words, we do not detect a difference in the reddening curves of arm and interarm regions. For some of the galaxies, the disparity between A_B and A_I is not as great as that in our own Galaxy, which has $A_B/A_I \approx 2$. Several of these galaxies have $A_B/A_I \approx 1.5$, so their extinction curves are flatter ("grayer") than the Galactic curve. Since our measurements are based on spatially averaged transmission values, the "effective" extinction may not be fully comparable to the extinction curves derived from what are essentially point sources in our own and nearby galaxies. In particular, since the dust distribution is directly observed to be clumpy on a wide range of scales, we may expect to see such a flattening of the observed extinction compared to that which would come from the intrinsic grain properties. Clumped extinction will saturate in B before I, which diminishes A_B/A_I. The more strongly clumped the dust, the flatter the extinction curve will be. In viewing a spatially extended region, the light at each wavelength comes preferentially from the areas with smallest extinction. As a simple example, if we consider a uniform dust screen with transparent holes that occupy some covering fraction η, the measured extinction curve from an extended background source will never give an effective extinction greater than $A = -2.5 \log \eta$, regardless of the optical depth in the screen; that is, if 10% of the area has no extinction, at no wavelength would we measure an extinction greater than 2.5 mag. We expect some conceptually similar (but naturally much more complex) situation to obtain in the disks of spirals. Our limited sample does not show any systematic difference in the slope of the effective extinction between arm and interarm regions or any overall trend with radius within the galaxies. In our analysis of additional observations, particularly *HST* imaging to trace the extinction structure to scales of order 10 pc (Keel & White 2000) and *Infrared Space Observatory* measurements to measure the overall dust masses (Domingue et al. 1999), we examine the role of clumpiness in more detail.

Our results bear on the question of whether the high-redshift "QSO cutoff" can be produced by absorption in spirals along the line of sight. The high redshift of the cutoff

offers plenty of room for even modest individual optical extinctions to have an impact, particularly if the effective extinction curve rises as steeply in the UV as the Galactic extinction curve does. For a fiducial set of spiral galaxy parameters, Ostriker & Heisler (1984) estimate that 50% of QSOs at $z = 4.5$ will suffer such obscuration by foreground galaxies; this is close enough to the characteristic peak redshift in the QSO distribution at $z \approx 2.2$ to make obscuration effects worth investigating. We find that disks are optically thin in spiral types Sb and later, which have $A_B < 1$ from 0.5 to 0.9 R_{25}; extinctions are generally below our measurement errors for $R > R_{25}$. The typical *interarm* behavior of our sample is similar to the model adopted by Ostriker & Heisler (1984), except that we find extinctions (at B) less than they assume by factors always greater than 2. Their fiducial model is based on the radial structure of the Milky Way and the integrated extinction perpendicular to its disk at the solar location $R_\odot$. Since we give our results in terms of R/R_{25}, we make contact with their results by noting that $R_\odot/R_{25} = 8$ kpc/11.5 kpc $= 0.7$ (following de Vaucouleurs & Pence 1978). This implies that the Ostriker & Heisler model has $A_B = 0.9$ at $0.5R_{25}$, in contrast to the $A_B = 0.1$–0.4 values we find for interarm regions at similar radii. Spiral arms will provide additional absorption, but they cover rather less than half the surface area in grand-design spiral disks. The covering fraction of spiral arms tends to be larger in flocculent spiral galaxies, however. Even given the uncertainties in the relative demographics of grand-design and flocculent spirals, the cumulative opacity from spiral galaxies is unlikely to be as large as in the fiducial model adopted by Ostriker & Heisler (1984). As noted by Fall & Pei (1993, 1995), the real situation is likely to be even more favorable for visibility of distant QSOs, since the dust abundance has almost certainly increased with cosmic time. Fall & Pei show that damped Lyα systems, the best candidates for absorption from disk gas, have dust-to-gas ratios that are factors of 4–16 below the usual Galactic value, supporting the notion of substantial chemical evolution since these epochs. From a more direct spectroscopic study, Lu et al. (1996) indeed find that abundances in high-redshift damped Lyα absorbers are quite low for $z = 1$–4 (3×10^{-3} to 0.1 solar) and increase significantly with cosmic time. These factors, abundance evolution and relatively more transparent interarm regions than initially assumed, suggest that dust obscuration cannot cause the deficit of high-z QSOs. While detailed calculations of this effect based on local galaxies may not be relevant to the high-z objects responsible for most of the cumulative extinction, we do note that a two-component model treating arm and interarm regions separately should reflect local reality much better than a single-zone scheme; most spiral arms are opaque enough to drop a QSO out of observed samples, but the half (or more) of a disk between dusty arms remains usefully transparent over much of the disk's projected area. Finally, QSO colors should redden with extinction in a more normal way than our diffuse-light extinction measures, since clumping of the dust can affect only extended background sources (which only the most extremely lensed QSOs would be).

The typical dust opacity is quite generally expected to show evolution with redshift, as stellar processing increases the cumulative dust mass over time (Pei & Fall 1995). Deep high-resolution data can eventually test this prediction, as we show with a feasibility test using images taken for the Hubble Deep Field–South (HDF–S) campaign (Williams et al. 2000; Gardner et al. 2000). The HDF–S STIS field includes a late-type spiral, seen highly inclined to the line of sight, partially projected in front of a face-on early-type spiral (Fig. 13), located at (2000) $\alpha = 22^h33^m39^s.9$, $\delta = -60°33'05''$. We have modeled this background object to estimate the extinction in the outer spiral arms of the foreground galaxy, using an interpolation of the brightness along the arm. For the 50CCD filter ("white light" from 0.3 to 1.1 μm weighted by the CCD response), we find the arm extinction to be only 0.1 mag (and it could exceed 0.2 only by an unfortunate coincidence of foreground light) over a region of about $0''.1 \times 0''.2$. What appear visually to be absorbing lanes on either side of this arm are mostly contrast artifacts; we find that they do not in fact show net absorption compared to the expected background intensity from a symmetric model. A spectrum of the blended light from these galaxies has been obtained by Glazebrook et al. (2000) and kindly made available via the World Wide Web. There is a spectral discontinuity near 6150 Å that would correspond to the 4000 Å break at $z \approx 0.55$, but neither K. Glazebrook et al. (2000, in preparation) nor we could find a strong cross-correlation peak (or pair of peaks) to refine this estimate. A redshift in this range does accord with the angular sizes of the galaxies and the red color of the background bulge, from comparison of the 50CCD and F20X50LP HDF–S imagery. While this spiral is of later type than would be expected to show higher extinction (and thus be most useful for tracing its redshift evolution), these data do show that such measurements are feasible as deep survey imagery accumulates.

We will report elsewhere on our studies of "peeking bulge" systems, in which the bulge of a nearly edge-on spiral backlights part of its own disk, since their analysis is more subtle. To avoid underestimating the optical depths in the intervening disks, one must be sure to scrape off the emission due to the intervening disk, which is difficult to estimate from the symmetric regions on the far side; furthermore, such systems are likely to have forward-scattered bulge light "fill in" much of the true absorption (see Byun, Freeman, & Kylafis 1994). Future papers in this series also include extension of the extinction curve coverage for some

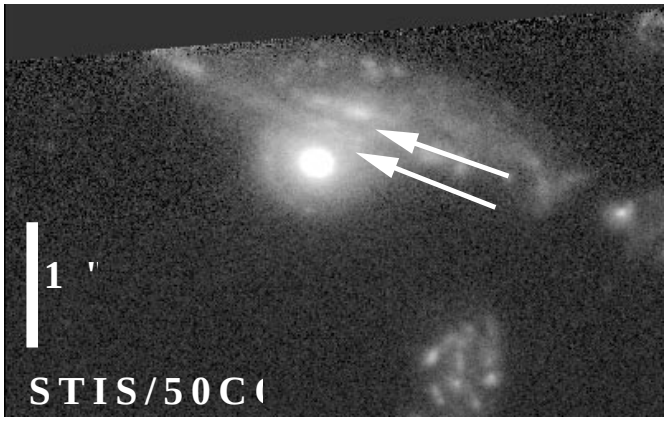

FIG. 13.—Overlapping galaxy pair found at the edge of the STIS field in the HDF–S, illustrated from the very broadband "white light" data in the S50CCD filter. The arrows mark the possible dust lanes in the foreground late-type galaxy. The background object is an early-type spiral with its own internal structure, so our modeling yields only modest upper limits to the extinction in these regions.

of these overlapping galaxies to U and K bands and the use of slit spectroscopy in overlapping regions to determine photon ownership by exploiting Doppler shift differences between overlapping galaxies (Domingue, Keel, & White 2000).

We thank Barry Madore for providing an electronic version of the AM catalog, greatly simplifying part of our search task. Duilia de Mello kindly obtained ESO redshifts of AM 1316−241 on our behalf. Mayo Greenberg and Adolf Witt updated our knowledge of the scattering parameters for grains. We acknowledge support from EPSCoR grant EHR-9108761 and NSF REU grant AST-9424226. R. E. W. was partially supported by a National Research Council Senior Research Associateship at NASA GSFC. We thank the director of Lowell Observatory for time to observe some of the pairs of especially large angular size, which formed an important complement to our KPNO and CTIO imaging. The Digitized Sky Survey was produced at the Space Telescope Science Institute under US Government grant NAG W-2166. The images of these surveys are based on photographic data obtained using the Oschin Schmidt Telescope on Palomar Mountain and the UK Schmidt Telescope. The plates were processed into the present compressed digital form with the permission of these institutions. The *HST* archival images were retrieved from the Space Telescope Science Institute, which is operated by AURA, Inc., under NASA contract NAS5-26555. We thank Karl Glazebrook for making the HDF–S spectrum available.

APPENDIX

SCATTERING CORRECTIONS

We attempt to calculate a maximum role for scattering as follows. We take the major-axis profile of the background galaxy and assume the galaxy to be circular with this profile as seen from each point in the foreground system. We further assume the dust to be uniformly distributed, as this is the most effective way to scatter light from a fixed amount of dust. Taking the geometry shown in Figure 14, we numerically integrate the intensity of scattered light as a fraction of the transmitted light, both normalized to the background intensity at the overlap position. We use the Henyey-Greenstein (1941) expression for the

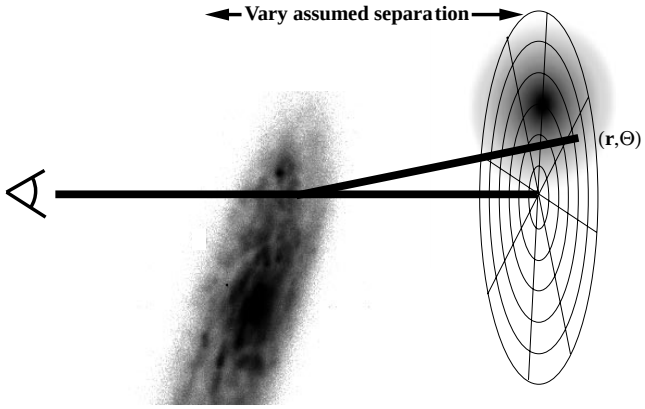

FIG. 14.—Schematic diagram showing the geometry and coordinate system used for calculating scattering correction. The relevant angle θ in the scattering phase function is evaluated between the projected line of sight into the background system and each point in the background galaxies, centered (as shown) on the point in the foreground system at which the line of sight passes through its disk (the location at which we are measuring the extinction). The center of the background galaxy is in the plane of the coordinate grid. Our numerical estimates assume a uniform dust screen in the foreground galaxy, which is the most effective configuration for scattering into the line of sight and thus furnishes an upper limit to the possible correction for scattered light.

TABLE 4

SCATTERING CORRECTIONS FOR OVERLAPPING PAIRS

Pair	Projection Radius (arcsec)	Minimum Separation/ Projection Radius	Scattering Fraction
AM 0500−620.....	6	9.0	0.03
AM 1316−241.....	6	8.5	0.01
AM 1311−455.....	52	3.6	0.05
NGC 1738/9	18	3.7	0.027
NGC 4567/8	39	5.5	0.04

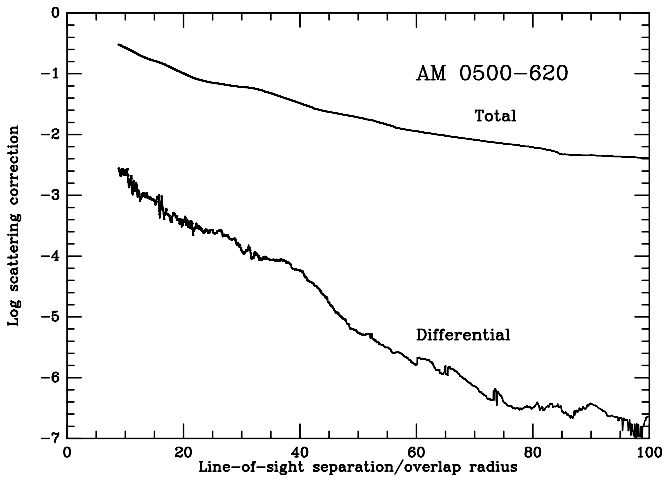

FIG. 15.—Sample plot of relative scattering intensity vs. assumed line-of-sight separation between the galaxies for AM 0500−620, calculated using the B profile of the background elliptical. Both total and differential scattering contributions are shown, to indicate how rapidly the differential correction (to which our technique is sensitive) drops with distance between the galaxies. The structure in the differential scattering curve reflects purely numerical fluctuations associated with the spacing of grid points with respect to radii at which the surface brightness profile is tabulated. The outermost symmetric isophotes suggest that the minimum allowed separation in the line of sight is 8 times the radius of the overlap region from the foreground nucleus. Even for the minimum plausible separation, the maximum role for scattered light is well within the errors of our extinction measurements.

phase function during scattering, which becomes

$$\frac{dI(r, \theta)}{I} = \frac{\tau a(1 - g^2)}{(1 + g^2 - 2g \cos \theta)^{1.5}}$$

in current notation; here I is the intensity of the background galaxy in the direction specified by r and θ, τ is the scaling by optical depth, a is the albedo at the relevant wavelength, and g is the asymmetry parameter. Based on the work of Witt, Oliveri, & Schild (1990), Witt et al. (1992), and Calzetti et al. (1995), we use $a = 0.6$ at both B and I, and $g = 0.8$. Since the line-of-sight separation is not directly known, we allow this to vary over the entire plausible range. For example, if neither pair member is morphologically distorted, the two galaxies probably do not physically overlap at the relevant radius. Figure 15 shows a sample calculation of scattering intensity for AM 0500−620. Both the total and differential scattering are shown on a logarithmic intensity scale, dropping rapidly with assumed separation as the background galaxy occupies a decreasing solid angle as seen from the scatterers. For galaxies more than a few radii apart, the effect becomes negligible (so we can ignore it for galaxies with very different redshifts). Scattering redistributes radiation in angle over the characteristic scale of the phase function, so that if one traces sharp features such as dust lanes, scattering will not affect the small-scale structure. This means that scattering is not important in those pairs where we use dust-lane or arm edges as the background tracers, as in UGC 2942/3 and NGC 3314.

We tabulate in Table 4 the adopted minimum plausible line-of-sight separation between galaxies for pairs in which scattering might be an issue, based on the outermost symmetric isophotes, and the maximum corrections for differentially scattered light at this separation. The table lists the projected distance between the innermost overlap region and the background nucleus, the minimum plausible line-of-sight separation between galaxies in units of this projected separation, and the calculated maximum differential scattered intensity as a fraction of the unabsorbed background light at the overlap location. The relative corrections (scaled to unit optical depth τ) are the same at B and I since we adopt a constant albedo across this wavelength range. As is apparent from the values in the table, the maximum corrections due to scattering are always less than a few percent in residual intensity, so that this is not a major uncertainty in our results.

REFERENCES

Andredakis, Y. C., & van der Kruit, P. C. 1992, A&A, 265, 396
Arp, H. 1966, Atlas of Peculiar Galaxies (Pasadena: Caltech); also in ApJS, 14, 1
Arp, H. C., & Madore, B. F. 1987, A Catalogue of Southern Peculiar Galaxies and Associations (Cambridge: Cambridge Univ. Press)
Berlind, A. A., Quillen, A. C., Pogge, R. W., & Sellgren, K. 1997, AJ, 114, 107
Block, D., Witt, A. N., Grøsbol, P., Stockton, A., & Moneti, A. 1994, A&A, 288, 383
Bosma, A., Byun, Y., Freeman, F. C., & Athanassoula, E. 1992, ApJ, 400, L21
Burstein, D., Haynes, M. P., & Faber, S. M. 1991, Nature, 353, 515
Burstein, D., Willick, J., & Courteau, S. 1995, in The Opacity of Spiral Galaxies, ed. J. I. Davies & D. Burstein (Dordrecht: Kluwer), 73
Byun, Y. I., Freeman, K. C., & Kylafis, N. D. 1994, ApJ, 432, 114
Calzetti, D., Bohlin, R. C., Gordon, K. D., Witt, A. N., & Bianchi, L. 1995, ApJ, 446, L97
Chatzichristou, E. T. 2000, ApJ, submitted (astro-ph/9912227)
Davies, J. 1990, MNRAS, 245, 350
de Mello, D. F., Keel, W. C., Sulentic, J. W., Rampazzo, R., Bica, E., & White, R. E., III 1995, A&A, 297, 331
de Vaucouleurs, G., et al. 1991, Third Reference Catalog of Bright Galaxies (Berlin: Springer) (RC3)
de Vaucouleurs, G., & Pence, W. D. 1978, AJ, 83, 1163
Disney, M. J. 1995, in The Opacity of Spiral Disks, ed. J. I. Davies & D. Burstein (Dordrecht: Kluwer), 5
Disney, M. J., Davies, J., & Phillips, S. 1989, MNRAS, 239, 939
Domingue, D. L., Keel, W. C., Ryder, S. D., & White, R. E., III. 1999, AJ, 118, 1542
Domingue, D. L., Keel, W. C., & White, R. E., III. 2000, ApJ, in press
Dreyer, J. L. E. 1888, New General Catalogue of Nebulae and Clusters of Stars, Mem. Roy. Astron. Soc. 49, Part I (reprinted 1953; London: Roy. Astron. Soc.)
Elmegreen, D. M. 1980, ApJS, 43, 37

Fall, S. M., & Pei, Y. C. 1993, ApJ, 402, 479
———. 1995, in QSO Absorption Lines, ed. G. Meylan (Berlin: Springer), 23
Gardner, J. P., et al. 2000, AJ, 119, 486
Henyey, L. G., & Greenstein, J. L. 1941, ApJ, 93, 70
Holmberg, E. 1958, Medd. Lunds Astron. Obs., 2, 136
Huizinga, J. E. 1994, Ph.D. thesis, Rijksuniv. Groningen
James, P. A., & Puxley, P. J. 1993, Nature, 363, 240
Karachentsev, I. D. 1972, Soob. S.A.O., 7, 3
Keel, W. C. 1983, AJ, 88, 1579
Keel, W. C., & White, R. E., III 1995, in The Opacity of Spiral Galaxies, ed. J. I. Davies & D. Burstein (Dordrecht: Kluwer), 167
———. 2000, ApJ, submitted
Knapen, J., Beckman, J., Jansen, R., Peletier, R., & Hes, R. 1995, in The Opacity of Spiral Galaxies, ed. J. I. Davies & D. Burstein (Dordrecht: Kluwer), 185
Kylafis, N. D., & Bahcall, J. N. 1987, ApJ, 317, 637
Lauberts, A. 1982, The ESO/Uppsala Survey of the ESO(B) Atlas (Garching: ESO)
Lu, L., Sargent, W. L. W., Barlow, T. A., Churchill, C. W., & Vogt, S. S. 1996, ApJS, 107, 475
McMahon, P. M., Richter, O.-G., van Gorkom, J. H., & Ferguson, H. C. 1992, AJ, 103, 399
Moles, M., Marquez, I., Masegosa, J., del Olmo, A., Perea, J., & Arp, H. 1994, ApJ, 432, 135
Nilson, P. 1973, Uppsala General Catalogue of Galaxies (Nova Acta Regiae Soc. Sci. Upsaliensis, Ser. V, A), 1
Ostriker, J. P., & Heisler, J. 1984, ApJ, 278, 1
Pei, Y. C., & Fall, S. M. 1995, ApJ, 454, 69
Pizagno, J., & Rix, H.-W. 1998, AJ, 116, 2191
Reduzzi, L., & Rampazzo, R. 1995, Astrophys. Lett. Commun., 30, 1
Reshetnikov, V. P., & Sazonova, L. N. 1993, Pis'ma Astron. Zh., 19, 708
Roennback, J., & Shaver, P. A. 1997, A&A, 322, 38
Rubin, V. C., & Ford, W. K., Jr. 1983, ApJ, 271, 556
Sandage, A., & Tammann, G. A. 1981, A Revised Shapley-Ames Catalog of Bright Galaxies (Washington: Carnegie Institution)
Schweizer, F., & Thonnard, N. 1985, PASP, 97, 104
Simien, F., & de Vaucouleurs, G. 1986, ApJ, 302, 564
Simien, F., Morenas, V., & Valentijn, E. A. 1993, A&A, 269, 111
Sinnott, R. W. 1988, NGC 2000.0: The Complete New General Catalogue and Index Catalogue of Nebulae and Star Clusters by J. L. E. Dreyer (Cambridge: Sky Publ. and Cambridge Univ. Press)
Sulentic, J. W., & Tifft, W. G. 1973, Revised New General Catalogue of Nonstellar Astronomical Objects (Tucson: Univ. Arizona Press)
Thronson, H. A., Jr., Rubin, H., & Ksir, A. 1991, MNRAS, 252, 550
Valentijn, E. A. 1990, Nature, 346, 153
van Houten, C. J. 1961, Bull. Astron. Inst. Netherlands, 16, 1
Vorontsov-Velyaminov, B. A., & Arkhipova, V. P. 1963, Morfologicheskii Katalog Galaktik, Vol. 3 (Moscow: Univ. Press)
———. 1964, Morfologicheskii Katalog Galaktik, Vol. 2 (Moscow: Univ. Press)
———. 1968, Morfologicheskii Katalog Galaktik, Vol. 4 (Moscow: Univ. Press)
———. 1974, Morfologicheskii Katalog Galaktik, Vol. 5 (Moscow: Univ. Press)
Vorontsov-Velyaminov, B. A., & Krasnogorskaya, A. A. 1962, Morfologicheskii Katalog Galaktik, Vol. 1 (Moscow: Univ. Press)
White, R. E., III, & Keel, W. C. 1992, Nature, 359, 129
White, R. E., III, Keel, W. C., & Conselice, C. J. 1996, in New Extragalactic Perspectices in the New South Africa, ed. D. L. Block & J. M. Greenberg (Dordrecht: Kluwer), 114
Williams, R., et al. 2000, AJ, in press
Witt, A. N., Oliveri, M. V., & Schild, R. E. 1990, AJ, 99, 888
Witt, A. N., Petersohn, J. K., Bohlin, R. C., O'Connell, R. W., Roberts, M. S., Smith, A. M., & Stecher, T. P. 1992, ApJ, 395, L5
Witt, A. N., Thronson, H., & Capuano, J. M. 1992, ApJ, 393, 611
Zhenlong, Z., Jiansheng, C., Xiaoying, T., & Yulin, B. 1989, Publ. Beijing Astron. Obs., 12, 8